Rho-Theta Parameterization for Color Blindness Image Segmentation

Yung-Sheng Chen, Long-Yun Li, and Chao-Yan Zhou

Abstract—**Segmentation of color information in RGB space is considered as the detection of clouds in rho-theta space. The conversion between RGB space and rho-theta space is first derived. Then the peak detection in the cloud-like rho-theta image is developed for color plane segmentation. The color blindness images are used for illustrations and experiments. Results confirm the feasibility of the proposed method. In addition, the segmentation of pattern and background for a color blindness image is also further demonstrated by means of the spatial distance computation among segmented color planes as well as the traditional *K*-means algorithm.**

Index Terms—**Color blindness image, image segmentation, RGB space, rho-theta space.**

I. INTRODUCTION

COLOR image segmentation is of great importance in the field of image processing and pattern recognition. It is known that the color visual perception from human eyes is primarily reflected by red (R), green (G), and blue (B) color components. Thus the constructed color space for color information processing is usually named as RGB space. In order to facilitate the specific applications, several color space conversion methods have been proposed. For example, CMYK (Cyan-Magenta-Yellow-Black) space is frequently used in color printer; HSI (Hue-Saturation-Intensity) space is often adopted for the investigation of human visual phenomena; Lab (L for lightness, a and b for color-opponent dimensions) can be regarded as a device-independent color space; and YUV space is used in the traditional video display. Jin and Li proposed a switching vector median filter based on the Lab color space converted from the RGB space [1]. Lee et al. investigated a robust color space conversion between RGB and HSI for date maturity evaluation [2]. Mukherjee et al. used YUV colors space for image demosaicing [3].

Several well-known methods have been developed for performing the image segmentation such as thresholding based on histogram, clustering, region growing, edge detection, blurring, etc, which can also be extended and applied for color image segmentation. Underwood and

Aggarwal projected the three-dimensional color space into two-dimensional plane and analyzed the color characteristics of detected tree outlines for reporting the degree of infestation present [4]. By means of the competitive learning technique, Uchiyama and Arbib presented a color image segmentation method which can efficiently divide the color space into clusters [5]. By combining region growing and region merging processes, Tremeau and Borel proposed a color segmentation algorithm [6]. Chen and Hsu adopted self-organizing feature map for performing color blindness image segmentation [7] and further developed an active-and-passive approach for understanding the figure in the color blindness image (CBI) [8].

Even there has a much progress in the field of color image segmentation during the past two decades, it still has a room for exploring the color space conversion on this topic. Since the CBI is often used for the investigation of human visual perception [8-11], in this study the CBI is adopted for investigating the characteristics between RGB space and a newly defined rho-theta space. Based on this new space, the segmentation of color information can be readily demonstrated.
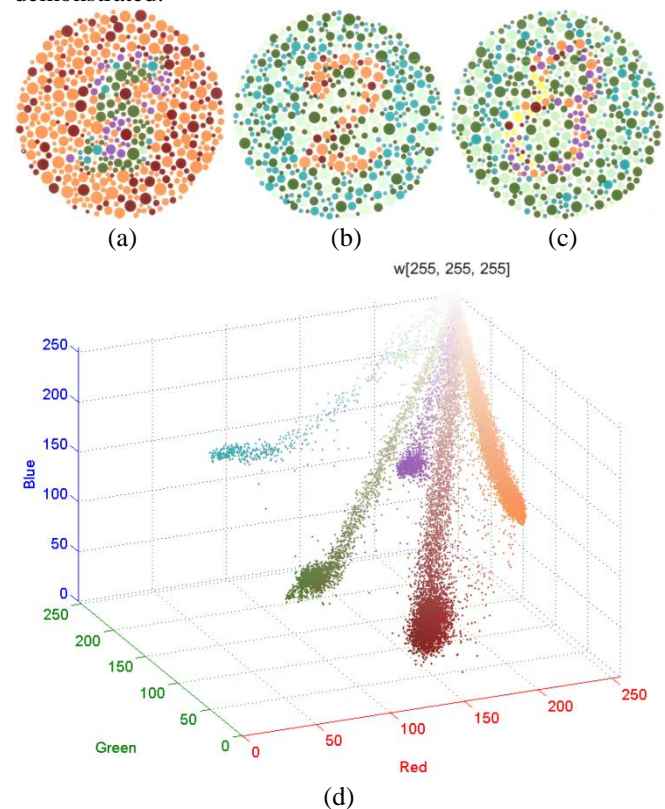

Fig. 1. (a)-(c) Three color blindness images from the Ishihara test plates, and (d) the color distribution in RGB space for CBI in (a), where five major color groups are easily observed.

II. Segmentation of Color Planes

A. Observation of a Color Image in RGB Space

Fig. 1(a)-1(c) show three CBIs, which are from the well-known Ishihara test plates and usually adopted for the study of color perception as mentioned previously. From our visual inspection, it mainly consists of the size-varied color dots with orange, brown, purple, green, and cyan colors. When it is used for the inspection of human color blindness, e.g., dichromats, the major colors will be focused on. In this case, the majority of color components are of red, whereas the minority is of green. For a normal vision, the figure "5" being composed of greenish dots can be perceived successfully, in which the majority of reddish dots is usually regarded as background. Note here that the white color is not used for perception and can be regarded as a reference.

Let a color pixel p including red, green, and blue components be denoted as $p[r, g, b]$. The color image in Fig. 1(a), for illustration, can be easily converted into the well-known RGB space and shown in Fig. 1(d). In this space, it is obvious that the color dots are mainly grouped into five color lines (i.e., purple, brown, orange, green, and cyan color lines) and separated from one to another. The concept of "color line" can be found in [12]. Therefore it is our goal in this study to develop a feasible method for the color segmentation method based on this observation.

B. Rho-Theta Space

Fig. 2 depicts the RGB space, where $o[0, 0, 0]$ represents the origin point or black point. However, as mentioned before, the white color can be regarded as a reference point, namely $w[255, 255, 255]$, in RGB space. This phenomenon can be found in Fig. 1(d), where the distribution of each grouped color line diffuses from the reference point to the space. Therefore, a rho-theta parameterization like scheme can be applied for this study. Consider a pixel $p[r, g, b]$ in RGB space, a vector can be constructed from reference point $w[255, 255, 255]$ to it. In this study, two parameters ρ and θ representing the included angle of $\overrightarrow{wp}$ and B-axis and that of $\overrightarrow{wp}$ and R-axis, respectively are used enough for further transformation. Ideally, each grouped color line distribution should be more gathered up in the new ρ-θ space. Based on this concept, the color segmentation could be readily performed in the ρ-θ space. According to the relationships in Fig. 2, the three components r, g, b of the pixel p can be represented as follows.

$$b = 255 - |\overrightarrow{wp}| \cos \rho \qquad (1)$$
$$r = 255 - |\overrightarrow{wp}| \cos \theta \qquad (2)$$
$$g = 255 - |\overrightarrow{wp}|\sqrt{1 - (\cos \theta)^2 - (\cos \rho)^2} \qquad (3)$$

where

$$|\overrightarrow{wp}| = \sqrt{(255 - r)^2 + (255 - g)^2 + (255 - b)^2} \qquad (4)$$

Thus we have

$$\rho = \cos^{-1}\left(\frac{255 - b}{|\overrightarrow{wp}|}\right) \qquad (5)$$

and

$$\theta = \cos^{-1}\left(\frac{255 - r}{|\overrightarrow{wp}|}\right) \qquad (6)$$

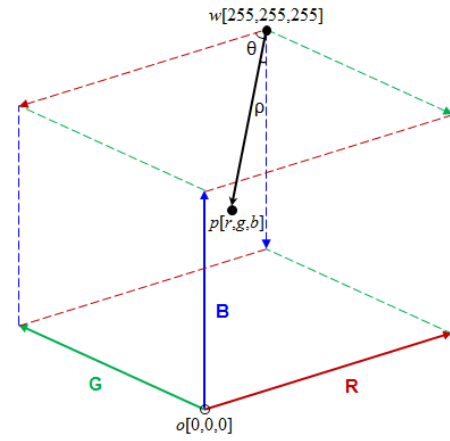to represent the so-called ρ-θ space.

Fig. 2. Illustration of transforming a color pixel from RGB space into ρ-θ space.

For the sake of performing the color segmentation, the ρ-θ space is designed as a two-dimensional array like the generalized Hough transform [13] uses. That is, if one case of ρ and θ occurs, it will be increased one in the memory location of (ρ, θ). The accumulated amount of (ρ, θ) indicates the number of those color pixels having ρ and θ values, which are treated as the same category as one color line in Fig. 1(d) displays. In order to make the color information to be more apparent for segmentation, all the pixels p having $|\overrightarrow{wp}| < 30$ (regarded as a white pixel) are ignored and will not be accumulated in the (ρ, θ) array, where the content at location (ρ, θ) is denoted as $C_{\rho\theta}$. The following procedure is next used for yielding the ρ-θ image. The threshold TH1 = 2 is selected experimentally in this study.

1) *For each memory location (ρ, θ), do steps 2-3.*
2) *Compute ρ_p, and θ_p for all color pixels p (not white).*
3) *If $|\rho - \rho_p| < TH1$ and $|\theta - \theta_p| < TH1$, then $C_{\rho\theta} \leftarrow C_{\rho\theta} + 1$.*
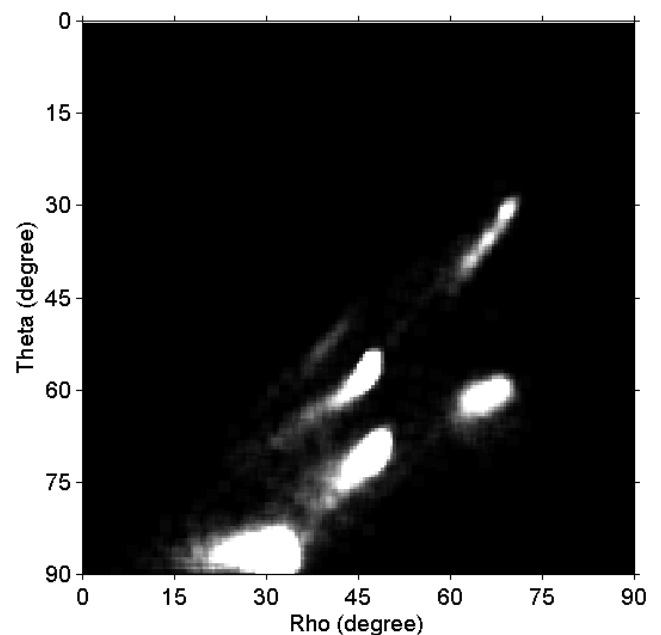

Fig. 3. Cloud-like ρ-θ image transformed from the RGB information in Fig. 1(d) by the proposed method.

Note here that the range of ρ and θ is within $[0°, 90°]$ and $C_{\rho\theta}$ is normalized with $\hat{C}_{\rho\theta} = C_{\rho\theta}/\bar{C}$, where $\bar{C}$ is the mean of all none-zero $(C_{\rho\theta})$s. Along this manipulation for Fig. 1(d), a cloud-like ρ-θ image can be obtained as shown in Fig. 3, where we can find five major groups (or clouds) containing brightness area as the five color lines indicated previously. In addition, one small-area group with less brightness is also shown. This cue is very helpful for the color image segmentation.

C. Find the Peaks in ρ-θ Image

According to the property of ρ-θ image, the segmentation of the groups can be transformed into finding the respective peaks. There are two steps, namely local maxima detection and small-peak removal, in this process, where a $(2s + 1) \times (2s + 1)$ sliding window is used. We adopted $s = 3$ for our experiments. In the step of local maximal detection, a peak is labeled if its value is the local maximum within the corresponding local area. Furthermore, there exist many unwanted small peaks which shall be ignored. In this study, only the peak having $\hat{C}_{\rho\theta} > (2T)^2/\bar{C}$ will be remained. After performing such a process on the ρ-θ image given in Fig. 3, eleven peaks are detected as shown in Fig. 4.
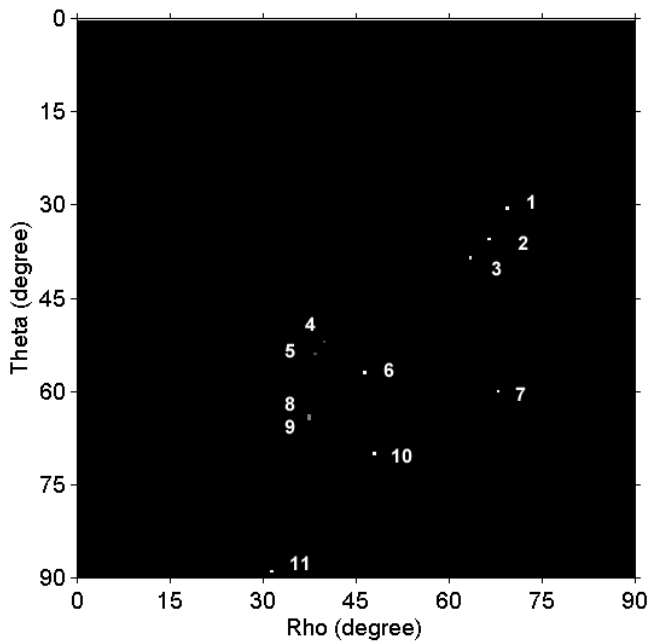

Fig. 4. Eleven peaks are found for the ρ-θ image given in Fig. 3.

By observing the images in Fig. 3 and Fig. 4, one cloud may include several peaks and one peak should have a local maximum within its cloud. In addition, the trend of pixel value changing is decreased gradually from the peak to the outer. Based on this property, we can use the relationship between any two peaks P and Q in the peak-image of Fig. 4 to represent whether they belong to the same group or not. Let v_P and v_Q be the value of peak P and Q respectively, PQ denote the line segment, and S_{PQ} be the set of all pixel values within the segment in the ρ-θ image of Fig. 3. In addition, note here that the value of "dark area" in Fig. 3 may not be exactly zero. Therefore a threshold $TH2 = \min(v_P, v_Q)/2.4$

is used in this study. Within any line segment PQ $(P \neq Q)$ we say peak P is not related to peak Q if there exists one pixel value belonging to S_{PQ} less than TH2. Otherwise, P and Q are related. After performing such an equivalent relationship process for Fig. 3 and Fig. 4, an equivalent relationship table can be obtained as given in Table I. Here peaks 1, 2 and 3 are regarded as the same cloud; peaks 4 and 5 the same cloud; and peaks 6, 8 and 9 the same cloud. Others (peaks 7, 10, and 11) are independent clouds. If several peaks are related, their maximal peak value can be used to represent the newly grouped peak. Fig. 5 shows the six peaks finally obtained from the current illustration.

TABLE I
EQUIVALENT RELATIONSHIP TABLE FOR THE PEAKS IN FIG. 4. HERE '1' AND '0' DENOTE WITH RELATIONSHIP OR NOT FOR TWO PEAKS.

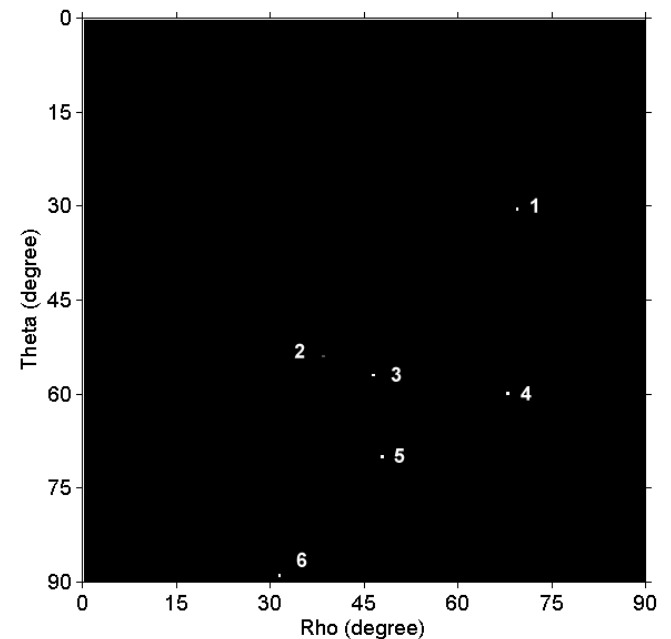| Peak	1	2	3	4	5	6	7	8	9	10	11
1	-	1	1	0	0	0	0	0	0	0	0
2	1	-	1	0	0	0	0	0	0	0	0
3	1	1	-	0	0	0	0	0	0	0	0
4	0	0	0	-	1	0	0	0	0	0	0
5	0	0	0	1	-	0	0	0	0	0	0
6	0	0	0	0	0	-	0	1	1	0	0
7	0	0	0	0	0	0	-	0	0	0	0
8	0	0	0	0	0	1	0	-	1	0	0
9	0	0	0	0	0	1	0	1	-	0	0
10	0	0	0	0	0	0	0	0	0	-	0
11	0	0	0	0	0	0	0	0	0	0	-

Fig. 5. Six peaks are obtained finally for the ρ-θ image given in Fig. 3.

D. Color Planes

According to the final six peaks shown in Fig. 5, we have six coordinates, $(\rho_i, \theta_i), i = 1, 2, ..., 6$, in the ρ-θ image. Since each RGB pixel has its (ρ, θ) based on (5) and (6), the pixel classification can be performed based on the distance between (ρ, θ) and (ρ_i, θ_i), i.e., $d(\rho, \theta; \rho_i, \theta_i)$.

If $d(\rho, \theta; \rho_k, \theta_k) = \min_{\forall i} d(\rho, \theta; \rho_i, \theta_i)$, then the pixel with (ρ, θ) is assigned to the class k. In the current illustration, there are six classes, and thus six color planes are

obtained as shown in Fig. 6. By observing these color planes in detail, there possibly exist some tiny noisy pixels (see Fig. 6(e) for example) which can be easily removed by means of the median filtering. Accordingly the final segmentation of color planes (namely 1, 2, …, 6 respectively) from the given CBI can be displayed in Fig. 7.
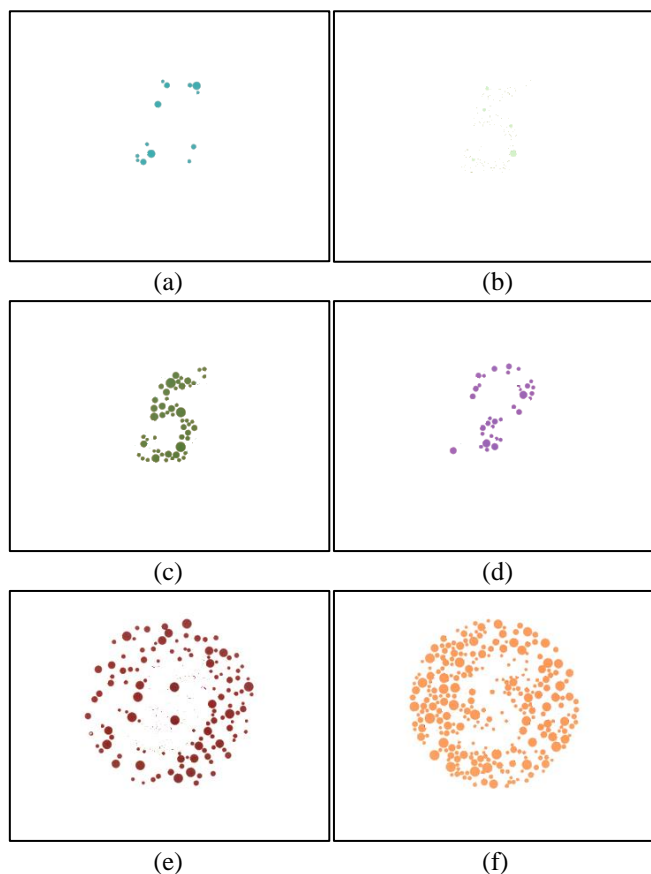

Fig. 6. Six color planes with color pixel assignment.

8(b), respectively.

Fig. 7. Six color planes (namely 1~6 respectively) after median filtering.

III. SEGMENTATION OF PATTERN AND BACKGROUND

In the case study of CBI, the CBI is usually divided into two classes, i.e., pattern and background, for further computer vision application [8, 11]. Even the main goal of this study has been achieved with rho-theta parameterization for color image segmentation, in this section a useful process of classifying pattern and background based on the found color planes will also be demonstrated for the further application. It mainly includes two steps: spatial distance computation between color planes [7] and classification using K-means [14]. By performing the spatial distance computation for the six color planes shown in Fig. 7, a symmetrical distance matrix can be obtained as given in Table II. It means that six 6-element distance vectors have been obtained. With the found distance vectors, it can be fed into the K-means algorithm to perform the clustering. Since only pattern and background will be classified in the current consideration, K is set to be 2. After the K-means computation, the color planes 1, 2, 3 and 4 are assigned to be the same class; whereas the color planes 5 and 6 the same class. Moreover since the number of pattern pixels is usually less than that of background pixels, the pattern and background are readily obtained as shown in Fig. 8(a) and

TABLE II
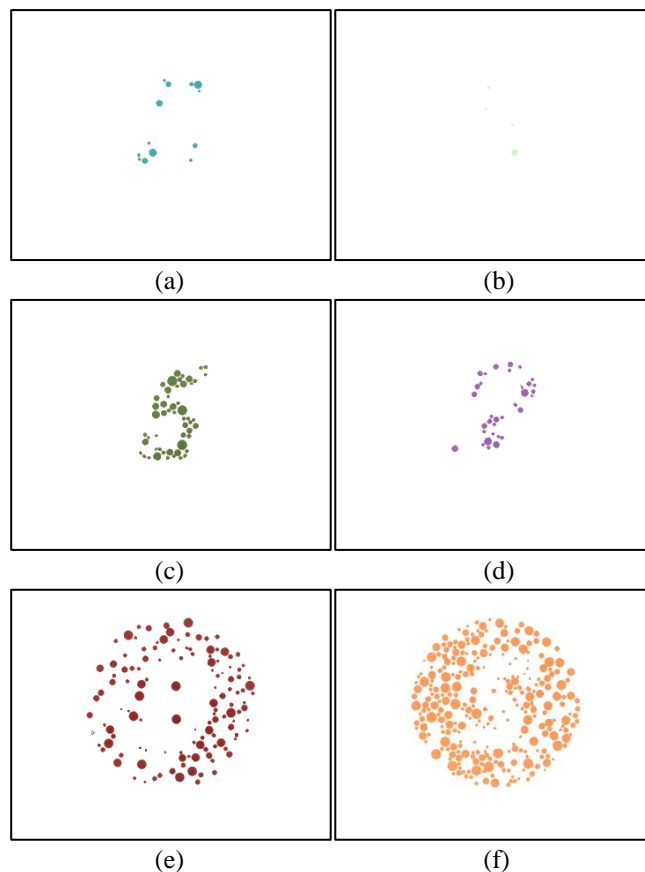SYMMETRICAL DISTANCE MATRIX OBTAINED BY THE SPATIAL DISTANCE
COMPUTATION FOR THE SIX COLOR PLANES SHOWN IN FIG. 7.

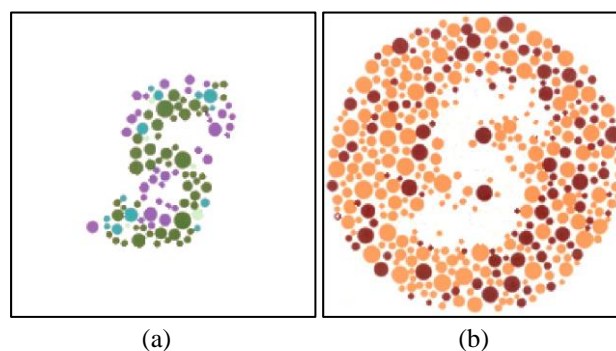| Color Plane	1	2	3	4	5	6
1	0.00	10.21	7.50	10.22	21.11	18.88
2	10.21	0.00	8.29	14.81	25.18	23.38
3	7.50	8.29	0.00	8.40	19.96	17.69
4	10.22	14.81	8.40	0.00	19.53	16.47
5	21.11	25.18	19.96	19.53	0.00	4.20
6	18.88	23.38	17.69	16.47	4.20	0.00

Fig. 8. Final segmentation of (a) pattern and (b) background for the CBI given in Fig. 1(a).
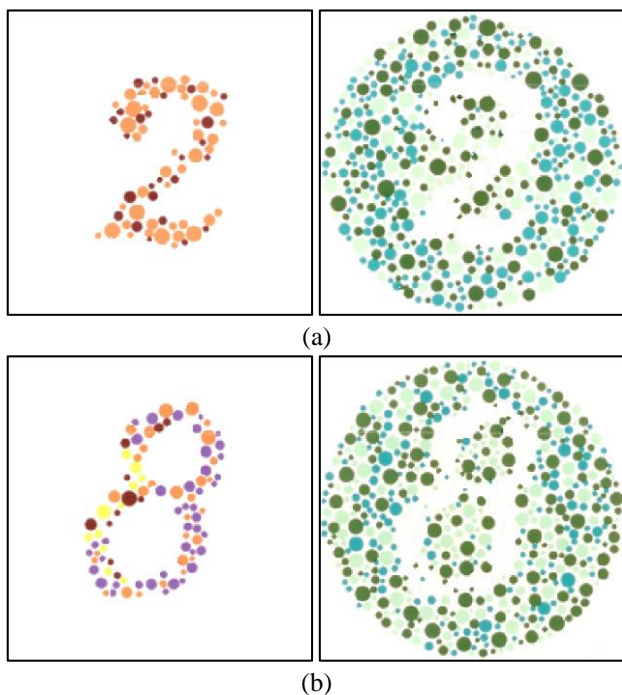
(a)

(b)

Fig. 9. (a) and (b) show the pattern/background segmentation results for the CBIs given in Fig. 1(b) and 1(c), respectively.

IV. RESULT AND CONCLUSION

Each CBI used in this study is of 196×196 pixels. The algorithm is implemented with MATLAB R2013a. Fig. 9 shows another two segmented results for the CBIs given in Fig. 1(b) and 1(c), respectively. The results confirm the feasibility of the proposed method. As a future work, in accordance with the concepts from color distribution to the cloud in rho-theta space, some manipulation schemes on the rho-theta space could possibly be developed for solving the wanted topics (like the detection of colored object and finding the relationship among colored objects in a color image) on the traditional RGB color space.

REFERENCES

[1] L. Jin and D. Li, "A switching vector median filter based on the CIELAB color space for color image restoration," *Signal Processing*, vol. 87, no. 6, pp. 1345–1354, 2007.
[2] D. J. Lee, J. K. Archibald, Y. C. Chang, and C. R. Greco, "Robust color space conversion and color distribution analysis techniques for date maturity evaluation," *Journal of Food Engineering*, vol. 88, pp. 364–372, 2008.
[3] J. Mukherjee, M. K. Lang, and S.K. Mitra, "Demosaicing of images obtained from single-chip imaging sensors in YUV color space," *Pattern Recognition Letters*, vol. 26, no. 7, pp. 985–997, 2005.
[4] S. A. Underwood and J. K. Aggarwal, "Interactive computer analysis of aerial color infrared photographs," *Computer Graphics and Image Processing*, vol. 6, no. 1, pp. 1-24, 1977.
[5] T. Uchiyama and M. A. Arbib, "Color image segmentation using competitive learning," *IEEE Transactions on Pattern Analysis and Machine Intelligence*, vol. 16, no. 12, pp. 1197 - 1206, 1994.
[6] A. Tremeau and N. Borel, "A region growing and merging algorithm to color segmentation," *Pattern Recognition*, vol. 30, no. 7, pp. 1191-1203, 1997.
[7] Y. S. Chen, and Y. C. Hsu, "Image segmentation of a color-blindness plate," *Applied Optics*, Vol. 33, No. 29, 6818-6822, 1994.
[8] Y. S. Chen, and Y. C. Hsu, "Computer vision on a colour blindness plate," *Image and Vision Computing*, vol. 13, no. 6, pp. 463-478, 1995.
[9] C.E. Martin, J.G. Keller, S.K. Rogers, and M. Kabrisky, "Color blindness and a color human visual system model," *IEEE Trans. Syst. Man Cyber.*, vol. 30, no. 4, pp. 494-500, 2000.
[10] T. Wachtler, U. Dohrmann, and R. Hertel, "Modeling color percepts of dichromats," *Vision Research*, vol. 44, no. 24, pp. 2843-2855, 2004.
[11] Y. S. Chen, C. Y. Zhou, and L. Y. Li, "Perceiving stroke information from color-blindness images," in *Proc. of IEEE International Conference on Systems, Man, and Cybernetics*, Budapest, Hungary, pp. 70-73, 2016.
[12] I. Omer and M. Werman, "Color lines: image specific color representation," in *Proc. of IEEE Computer Society Conference on Computer Vision and Pattern Recognition*, vol. 2, pp. 946-953, 2004.
[13] R. O. Duda and P. E. Hart, "Use of the Hough Transformation to Detect Lines and Curves in Pictures," *Comm. ACM*, vol. 15, no. 1, pp. 11–15, 1972.
[14] J. MacQueen, "Some methods for classification and analysis of multivariate observations," in *Proc. Fifth Berkeley Symp. on Math. Statist. and Prob.*, Univ. of Calif. Press, vol. 1, pp. 281-297, 1967.